

Illustration of Capacity Fading Factors on the Example of La₂(Li_{0.5}Ni_{0.5})O₄-Modified High Nickel Layered Oxide Material

Irina A. Ivanishcheva,^[a] Aleksandr V. Ivanishchev,^[a] Joon Ha Chang,^[a] Jung-Hoon Song,^[a] Su-Hyun Lee,^[a] Jae-Joong Kim,^[a] Young Je Kim,^[a] and Sang-Cheol Nam^{*[a]}

Modifying of layered oxide NCM ($\text{LiNi}_{0.85}\text{Co}_{0.1}\text{Mn}_{0.05}\text{O}_2$) with high nickel (Ni) content is a popular strategy for development of energy-dense cathode materials for LIBs. In spite of long-time investigations of their electrochemical performance there is no clear understanding of the predominant capacity fading reasons as well as the mechanism of suppression of performance degradation for modified samples. In the present work, NCM (bare and washed) powders were modified by perovskite-like phase La₂(Li_{0.5}Ni_{0.5})O₄ (LNP), using lithium residual compounds (LRC) from NCM surface. Initial properties of NCM-materials

were under our focus in terms of structural data of pristine powders and the first cycle capacity loss. We observed that incomplete lithium extraction in case of LNP-modified NCM bare sample preserves electrochemical performance. For illustration of the main reasons of capacity fading new type Δ -plots were proposed. Based on their analysis we highlighted two factors, affecting on capacity retention. Our conclusions were supported by D vs. E dependence analysis from GITT measurements.

Introduction

The interest towards Ni-rich transition metal oxides is motivated by their high specific capacity. However, the main problems of their application in LIBs (lithium-ion batteries) still require the intensive research work for comprehensive understanding the processes occurred during this type of cathode material operation. The ways to fix degradation problems should be simple and cost-effective owing to its long-time commercialization and large-scale production. From this point of view, the scientific work should focus at easy to perform modification route, based on coating ready-made NCM powder by different types of compounds.

The choice of surface modifier depends on proposed degradation mechanisms. For layered oxide structure cathode materials, degradation could be caused by bulk structural changes, e.g., undesirable phase transition accompanied by anisotropic volume change, cation disordering, cracking and surface instability effect (gas evolution, metal dissolution, surface impurities from Li-residuals and impedance built up).^[1–5] Coating compounds can act as barrier for undesirable process, such as oxygen releasing, transition metal displacement from structure, or as a conductor for lithium ions flux.^[6–8] Some of them can possess surface structure stabilizing and cracking suppress properties. Basically, the improvement for coated materials can be expressed in terms of capacity stabilization.^[9–12] But sometimes, increasing of discharge ca-

pacity level is observed as well.^[13] Most investigations are devoted to material surface problems.^[14,15] Nowadays, researchers concentrate on the issue of designing a functional interfacial layer and studying its impact on suppressing the parasitic reactions between the delithiated cathode and the electrolyte solution. Based on the difference in surface chemistry, Phillip et al.^[16] explained the effect of acid-base nature of oxide coatings on cathode performance through cathode electrolyte interphase (CEI) composition. Others depicted the doping effect of metal from coating layer as well.^[17–21] The Myung group^[22] summarized the early papers on the role of coating layer and concluded that it didn't suppress the structural changes of layered oxides during cycling but effected on interfacial properties on substrate material surface.

The object of our investigation was the cathode material powder: high Ni layered oxide cathode material NCM (Ni content is 85%, Co 10%, Mn 5%). Ni-rich layered oxides suffer from an abrupt anisotropic lattice volume change in the deeply charged state. Unfavorable phase transition leads to the appearance of NiO rock-salt-like layer on particle surface, which triggers other detrimental processes.^[23] Layered oxide surface, pinned by inactive NiO, were under investigation.^[24] They observed three phases with different lithium contents and concluded that the origin of the fatigue degradation is the high lattice strain at the interface between surface and bulk at highly delithiated stage. Some previous works^[25,26] demonstrate that capacity loss depends on concentration of rock-salt domain, and decreasing of Li ion mobility is caused by incremental cation mixing in the bulk. It was concluded that the observed surface reconstruction, on the one hand, means a loss of CAM (cathode active material), which results in an irreversible capacity loss.^[27] On the other hand, it causes a significant overpotential thereby shrinking the apparent SOC (state of

[a] Dr. I. A. Ivanishcheva, Prof. A. V. Ivanishchev, Dr. J. H. Chang, Dr. J.-H. Song, S.-H. Lee, J.-J. Kim, Y. J. Kim, Dr. S.-C. Nam
Research Institute of Industrial Science and Technology (RIST)
POSCO Global R&D Center
100 Songdogwahak-ro, Yeonsu-gu, Incheon, 21985 (South Korea)
E-mail: scnam1203@rist.re.kr

charge) window. The fact that part of the cathode material stays electrochemically active just in limited lithium concentration is observed in different types of cathode materials: LCO (irreversibility phase transformation at high cut-off voltage^[28]), LVP (lithium diffusion provides by two kind of Li⁺ – high mobile and low mobile Li-ions^[29]), LFP (formation of inactive zone inside particle at charging^[30]). All these works are based on labor-intensive studying and long cycling experiments. Owing to their results, the origin of degradation mechanism became clearer, and numerous modifying techniques for suppression of undesirable transformation, resulting in capacity fading, are currently keeping on sight.^[31–33] It is customary to examine electrochemical properties based on cycle-life behavior, presented in terms of capacity retention (in %). The longer cycling test, the more reliable results and the more accurate prognosis of capacity level at different states of electrode cycle life. Such measurements are accompanied by time consumption. At this paper we present fast and relatively simple approach for estimation of dominant degradation factors, which influence on electrode performance. It can be used for comparison of different modified NCM-based cathode materials. Short cycling test (instead of several hundred cycles) allows to reduce the time of comparative investigation of modified and non-modified materials but not at the cost of informativity.

For this purpose, four samples were explored in charge/discharge galvanostatic mode, limited by 50 cycles. One sample was bare (NCM_B) and one sample underwent washing procedure of bare powder (NCM_W). Additionally, these two samples were surface treated to create Li₂(La_{0.5}Ni_{0.5})O₄-modified cathode materials: LNP-NCM_B and LNP-NCM_W. The K₂NiF₄-type structure of modifier is related to the perovskite type structure. Similar to the perovskite phase (La, Li)TiO₃, K₂NiF₄-type La₂(Li_{0.5}Me_{0.5})O₄ (Me=Mn, Co, Ni) was reported to have high conductivity; La₂(Li_{0.5}Ni_{0.5})O₄ – mixed conductor with dominant electronic component of conductivity (up to 10⁻¹ S cm⁻¹ at room temperature).^[34] La₂(La_{0.5}Ni_{0.5})O₄-phase is mainly formed by the reaction between La- and Ni-containing species, on the surface of NCM during the heat-treatment at high temperature in oxygen atmosphere.^[35,36] Modification of layered oxide cathode materials by La₂(Li_{0.5}Ni_{0.5})O₄ and the reasons of capacity fading were presented in many literature sources.^[36–42] The improved performance of LNP-coated cathodes is attributed to the enhancement of structural stability resulting from increased conductive properties (both electronic and ionic transport) of modified electrodes.

Results and Discussion

The powder XRD patterns (Figure 1) reveal that all samples have a hexagonal α -NaFeO₂-type structure belonging to the R3m space group (166). It indicates that the surface modification doesn't affect the crystal structure of LiNi_{0.85}Co_{0.15}Mn_{0.05}O₂. In case of LNP-modified powders, the presence of La₂(Li_{0.5}Ni_{0.5})O₄-phase was detected. The four diffraction peaks of LNP-modified powders in the range of 2 θ -angle from 20° to 35° are assigned to Cmmm (65) space group, while non-modified NCM samples (bare and washed) do not display any characteristic peak at these positions (Figure 1d). The Rietveld refinement results are presented in Table 1. Referring to XRD data essentially there is no difference in bulk structure of all pristine samples at their starting points of electrochemical testing. The cell lattice parameters' variation is at the range of $\pm 0.1\%$ (Table 1). It is expected that electrochemical properties of our samples will be close to each other. Only LNP-NCM_W sample demonstrates increased c lattice parameter and the highest level of Li/Ni disordering. Integrated intensity ratio $I(003)/I(104)$ points on high degree of cation mixing.^[43] As the formation of La₂(Li_{0.5}Ni_{0.5})O₄-phase involved lithium ions consumption and washed powder contained the lowest amount of LRC, so it can be possible that rather NCM structure served as Li-source, than LRC. In this case, Li⁺ removing from NCM_W structure leads to partly Ni²⁺-ions migration in lithium ions layer due to close ionic radii.^[44] Furthermore, for LNP-NCM_W sample, the spacing between the peaks in the (108)/(110) doublets increases comparing to other samples (Figure 1c). Increasing the distance between (108) and (110) peak positions can be interpreted by partly chemical delithiation of the NCM bulk structure occurred during La₂(Li_{0.5}Ni_{0.5})O₄-phase formation on layered oxide substrate. In contrast, in case of LNP-modification of NCM_B the (003) peak shifting to higher angle, attributed to c-lattice decreasing, depicts on some recovery process during sample treatment (Figure 1b).^[45]

At the same time, not only LNP-NCM_W electrode has high degree of cation mixing, but all other samples are characterized by $I(003)/I(104) < 1.2$, that means more than 6% Ni in Li positions.^[46] Nonetheless, capacity retention behavior of all cells are quite different with different tendency at room temperature (RT) and elevated temperature (HT) and doesn't correlate with Li-Ni mixing. As reported,^[27] at long-term cycling, cation mixing stays at the same level and does not contribute to capacity loss. So, cation mixing cannot be considered as substantial factor for cycling performance. Moreover, some researchers

Table 1. The Rietveld refinement results for pristine modified and non-modified NCM samples.

Sample	a/b [Å]	c [Å]	V [Å ³]	c/a	$I(003/104)$	$T_{\text{TO}6}$ [Å]	$T_{\text{LO}6}$ [Å]	Phase content [%]	R_{wp} [%]	GoF
NCM_B	2.8714	14.1888	101.309	4.9414	1.1344	2.1378	2.5918	100 (R3m)	8.57	2.85
LNP-NCM_B	2.8695	14.1860	101.160	4.9437	1.1242	2.1515	2.5772	99.25 (R3m) 0.75 (La ₂ Li _{0.5} Ni _{0.5} O ₄)	8.92	3.95
NCM_W	2.8705	14.1898	101.256	4.9433	1.1453	2.1436	2.5863	100 (R3m)	7.47	2.46
LNP-NCM_W	2.8710	14.2039	101.392	4.9474	1.1161	2.1940	2.5406	99.30 (R3m) 0.70 (La ₂ Li _{0.5} Ni _{0.5} O ₄)	8.29	3.69

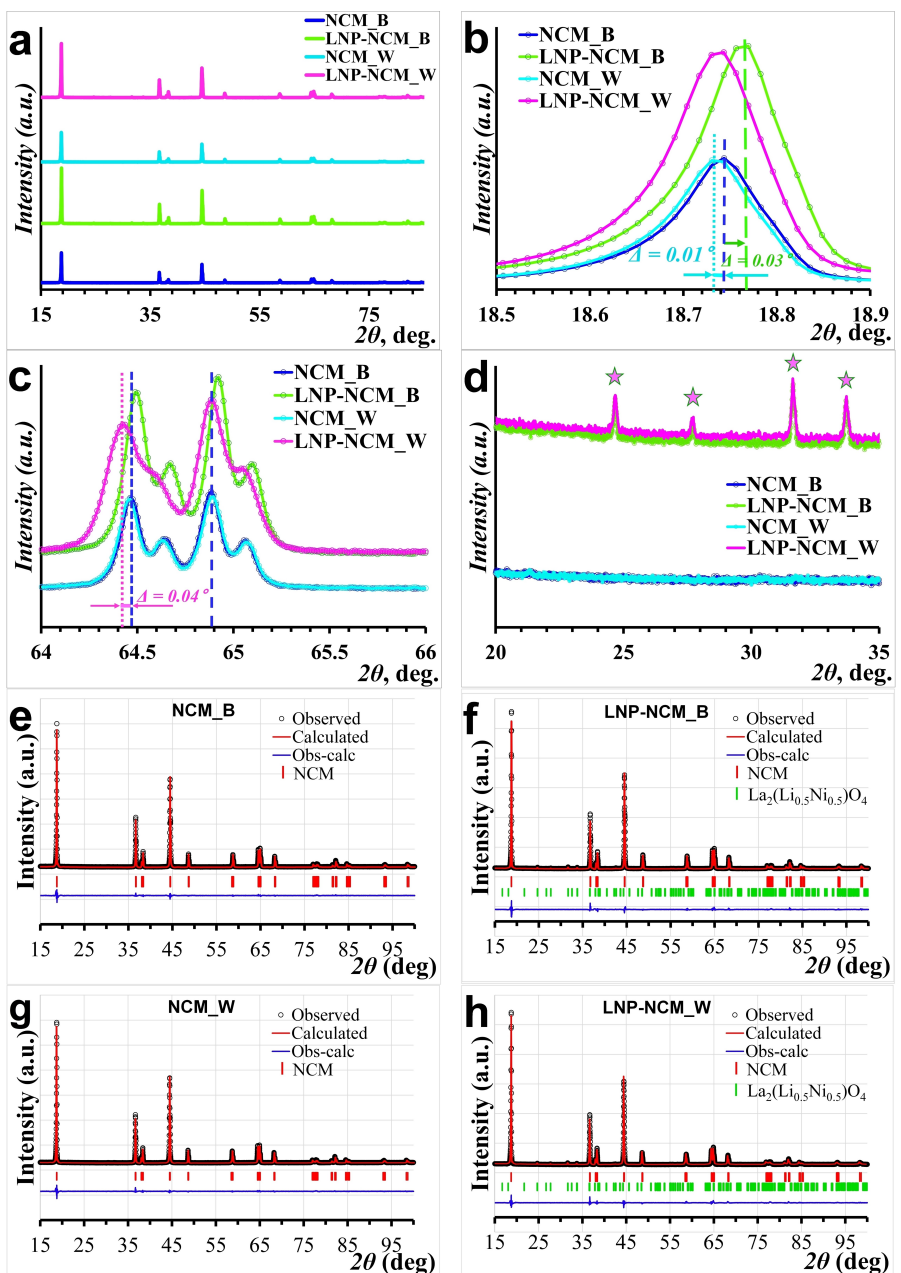


Figure 1. a) XRD patterns for all pristine powders; b–d) fragments at different 2θ -ranges. Peaks for $\text{La}_2(\text{Li}_{0.5}\text{Ni}_{0.5})\text{O}_4$ -phase are marked by asterisks in (d). e–h) Observed versus calculated curves for all samples.

reported about creation surface pillaring layer with Ni in Li-positions, suppressing interslab collapse during cycling and improving cell cycle life.^[47,48] From this viewpoint, more reliable estimation of samples' cycle life can be performed by analysis of the thickness of interslab distance. The corresponding columns in Table 1 present the thickness of octahedra layer with Li or transition metal inside, calculated by z_{ox} -value and c lattice parameter. In both substrate cases (bare and washed samples), the thickness of TMO_6 -slab increases and LiO_6 decreases after modifying by $\text{La}_2(\text{Li}_{0.5}\text{Ni}_{0.5})\text{O}_4$ -phase, that should have resulted in worsening of cycling properties due to contraction of free Li^+ -ions diffusion space. The fact that the first discharge capacities of NCM_B and NCM_W are higher

than one for LNP-modified samples confirms tendency of TMO_6 - and LiO_6 -slab variation among the samples. However, at extended cycling we observe improvement of capacity retention for LNP-NCM_B samples, which is significant in case of elevated temperature. This contradiction can be explained by some other factors. So, we conclude that within the reasonable variation range, structural data of pristine cathode powders cannot unambiguously predict their electrochemical performance.

It should be noted that bare material has higher content of lithium contained species formed from Li-sources and storage atmosphere surroundings (Table 2) comparing to washed powder. The fact that lithium residual compounds create

Table 2. The residual lithium content of the pristine NCM_B and NCM_W powders, determined by acid titration.		
Substance	NCM_B	NCM_W
Li ₂ CO ₃ [ppm]	10255	4829
LiOH [ppm]	3900	1503
Total LRC ^[a] [ppm]	14155	6332
[a] Lithium residual compounds.		

barrier layer for lithium ions intercalation/deintercalation is well-known from many publications.^[15,49,50] That is why washing (sometimes with some additives in solution) is a popular strategy to stabilize electrode characteristics. Accurate removing of lithium residual compounds from the surface is able to get from material its possible characteristics. At the same time, washing procedure detriments outer layer of material resulted in cells performance deterioration upon cycling.^[15] From Table 3, initial capacities of washed sample, measured at RT, are relatively higher comparing to bare samples, but cycling

experiment shows that NCM_W electrodes have higher degradation tendency (Figure 2a, b).^[51–53]

The reasons of this phenomenon are discussed in literature and can be shortly listed as Li⁺/H⁺ exchange at nearby surface region,^[54] formation of oxygen-depleted and more resistive surface layer,^[55] worsening in Ni/Li disordering,^[43] activation of surface reconstruction into the rock-salt phase.^[15] However, at 45 °C we observed decreasing of capacity loss during cycling (Figure 2c) for washed sample. Elevated temperature promotes more intensive interaction of “pure” NCM-surface with electrolyte components that creates protective CEI. CEI formation leads to uniform thin passivation layer distribution, isolating material bulk from electrolyte attacks, and thereby improving of capacity retention (88% for NCM_W-electrodes vs 84% for NCM_B after 50 cycles at 45 °C) (Figure 2d).

The composition of CEI is a variety of organic and inorganic components and their role for electrode material performance is significant: they can as impede electrode transport properties due to high resistance as, once upon at initial charge, they can

Table 3. Initial electrochemical performance at room and elevated temperature (0.1 C, 3.0–4.3 V).

Test temperature [°C]	Sample	The 1-st cycle capacity [mAh/g]			Coulombic efficiency (the 1-st cycle) [%]	The 2-nd cycle capacity [mAh/g]		Coulombic efficiency (the 2-nd cycle) [%]
		Charge	Discharge	Cap.loss ^[a]		Charge	Discharge	
25 (RT)	NCM_B	219.3	193.5	25.8	88.2	199.8	200.3	100.3
	LNP-NCM_B	207.3	178.2	29.1	86.0	185.2	184.9	99.8
	NCM_W	221.1	199.5	21.6	90.2	205.2	203.4	99.1
	LNP-NCM_W	222.8	193.1	29.7	86.7	197.1	197.5	100.2
	NCM_B	226.7	214.2	12.5	94.5	215.9	216.4	100.2
	LNP-NCM_B	225.7	209.6	16.1	92.9	211.3	212.2	100.4
	NCM_W	226.3	215.5	10.8	95.2	217.3	215.5	99.2
	LNP-NCM_W	226.6	211.4	15.2	93.3	213.1	214.5	100.7

[a] Difference between charge and discharge capacities.

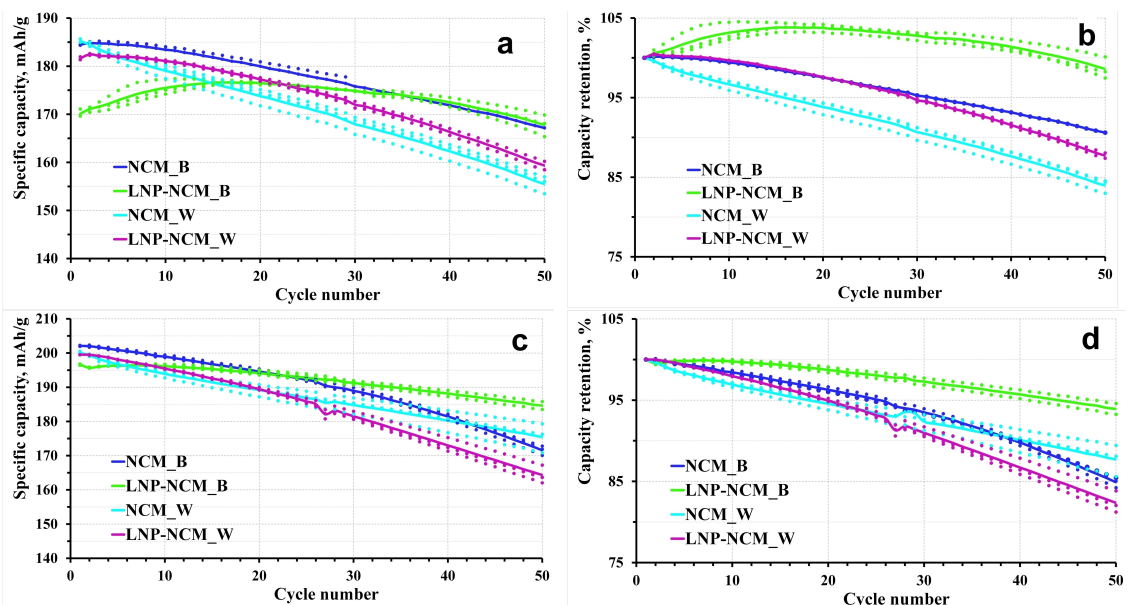


Figure 2. Galvanostatic charge/discharge cycling performance at 1 C (3.0–4.3 V). a, c) Specific discharge capacity, b, d) capacity retention. Upper curves correspond to characteristics, measured at 25 °C, lower curves – at 45 °C.

protect electrode material from further degradation caused by electrode material – electrolyte interaction.^[14,56,57] That is why the simple washing procedure, aimed at removing of lithium excess trace from surface, became popular. So, we found that washing treatment is quite reasonable procedure in case of elevated temperature operated electrodes.

Obviously, that LNP-modified samples have extraneous submicron-sized particles at NCM-particles' surface. They have rounded shape and are distributed between primary NCM-particles, forming so called "island-coating" (Figure 3d, h).^[58]

As all modified powders were heat treated before electrode mass preparation, their initial state is expected to be different from non-modified samples. Heat treatment itself has strong influence of layered oxide material properties^[50,59] and at the presence of modifier raw compounds (La and Ni metal salts in our case) the *in situ* modification should result in distinguished characteristics of material. However, charge capacities of the first cycles are approximately equal for set of samples at certain temperature (≈ 221 mAh/g for RT and ≈ 226 mAh/g for HT), that depicts on the same state of pristine electrodes (modified and non-modified). In spite of almost the same charge capacity

values, we observe the variation of discharge capacities among the samples since their first cycle (Table 3). Specific capacities of the first cycle for LNP-NCM_B are lower than others.

The problem of the first cycle capacity loss has been known for a long time.^[60–62] Generally, the first capacity loss (≈ 30 mA/g) of layered oxide materials is classified into reversible loss (can be recovered) and irreversible loss (< 3 % of total discharge capacity^[60,61]).

The reversible capacity loss can be explained in view of D_{Li^+} vs E dependence (Figure 4). We present the results of GITT measurements, performed accordingly to procedure, described earlier.^[29] Essentially, there is no difference in lithium transport properties of all NCM materials as it needs to be. D is intrinsic characteristic of bulk of material, related to its structure. As we have the same NCM layered oxide phase in our samples, it is expected that their D values will be very close to each other. But there is one aspect regarding the D evolution on E. We have different start points in each measurement directions: in charge direction the initial state is fully occupied Li-position structure and in discharge direction the initial state is totally empty Li-positions in the bulk. In discharge direction abruptly decreasing of D_{Li^+} at fully lithiated state (at < 3.6 V) implies that at the end of discharge there is deceleration of lithium movement (corresponds to $D \sim 10^{-15}$ cm²/s), resulting in incomplete Li-ion insertion. In contrast, charging starts right from high D values ($\sim 10^{-13}$ cm²/s) and proceeds at almost constant diffusion rate, providing full delithiation. The difference of lithium content in material's structure at the end of one-direction process, caused by different Li-ions diffusivity, we ascribe to reversible capacity lack. The temperature growth allows to extend lithium extraction range without structural stress. For example, almost 100 % of first capacity loss was recovered at 40 °C due to slow constant voltage discharge mode (cut-off voltage is 4.3 V).^[63] In our case (without applying constant voltage discharge mode) at temperature rising (up to 45 °C) almost half of capacity loss at RT are still not restored in the first cycle (Table 3). The very fact of temperature influence indicates that the first cycle capacity loss is predominantly under the kinetic control.

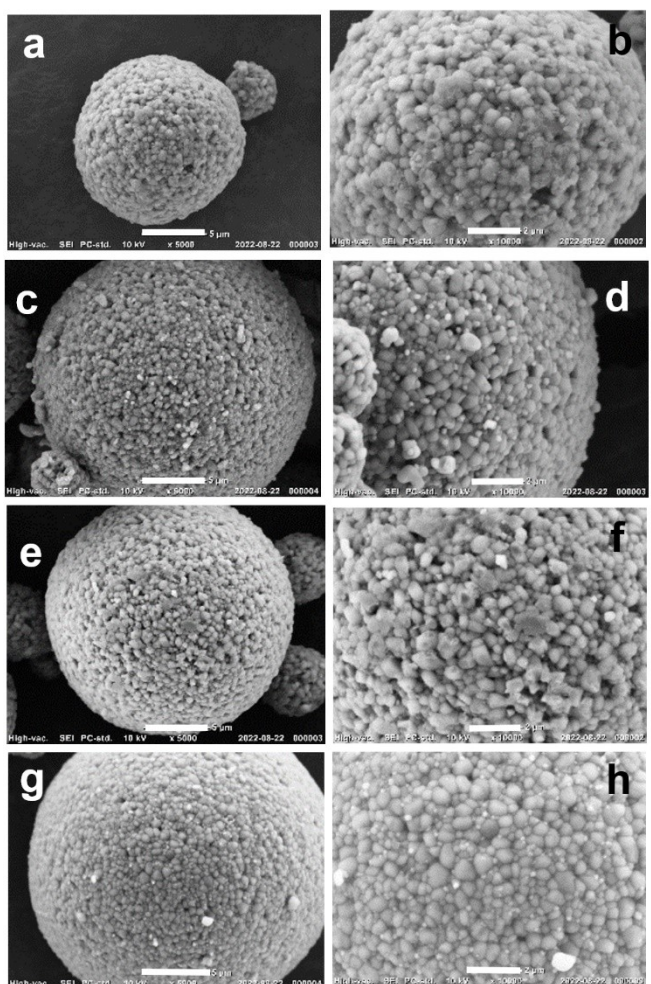


Figure 3. SEM images of a, b) NCM_B; c, d) LNP-NCM_B; e, f) NCM_W; g, h) LNP-NCM_W. Scale bars correspond to 2 μ m (right side) and 5 μ m (left side).

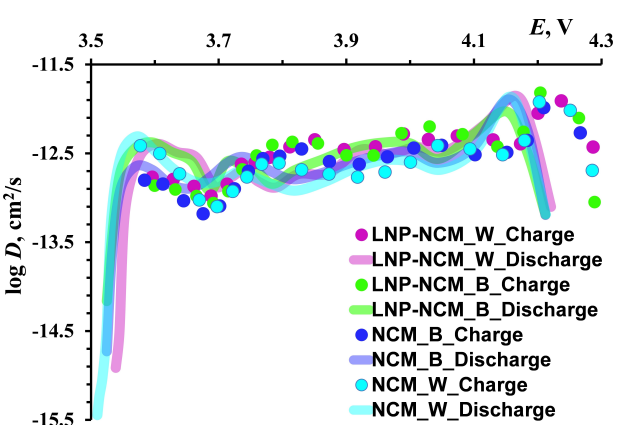


Figure 4. Dependences of the Li^+ diffusion coefficient in NCM_B, LNP-NCM_B, NCM_W and LNP-NCM_W on the electrode potential.

The irreversible capacity loss is generated by blocking of Li diffusion pathways, arising from surface structural instability and detrimental phase transformation into inactive NiO-phase. Local collapse of the interslab space due to the presence of nickel ions in the lithium layers additionally restricts Li-insertion.^[64] This capacity cannot be recovered. From the second cycle the columbic efficiency in our experiments is close to 100% (Table 3).

As described in Experimental section we did not use any Li-sources for creating LNP-modified samples. Instead of it we expected utilization of lithium residual compounds on NCM surface.^[36,39,41,65] Based on target content of coating compound in NCM substrate material – 1% by weight – we mixed appropriate amounts of La- and Ni-salts. Nevertheless, it is clear that only 0.7% of LNP-coating was reached (Table 1). It means that part of metal sources, mainly Ni-compound (as its mole ratio to La is 1:4), was unconverted to target phase. As it is difficult to detect so small content (less than 0.7%), we assume that remaining portion of Ni-raw compound reacted with O₂ at heat treatment stage to produce NiO in NCM-modified powder. Such kind of conversion we observed during separate La₂(Li_{0.5}Ni_{0.5})O₄-phase synthesis experiment (not presented here). This extra NiO-phase was not generated during degradation in layered oxide materials at cycling, but artificially introduced into NCM particles surface at final step of modified materials preparation. The thermodynamic aspect of NiO presence – low Gibb's free energy (-211 kJ/mole) – confirms this hypothesis. Cycling behavior of LNP-NCM_B at room temperature represents non-monotonic curve with maximum at the 20-th cycle (Figure 2a, b). Exploitation of electrode active mass, occurred at initial 20 cycles, we assign to the presence of artificially introduced with coating material NiO-phase, directly attached to NCM-substrate surface. Since LNP-NCM_B powder were prepared without washing stage, extra NiO-phase presences upon lithium residual species layer and mostly is separated from NCM surface by LRC layer. The adhesive force, providing blocking of NCM surface by this NiO-insulator, becomes weaker from cycle to cycle. And realized discharge capacity value increases. Parallel to this transformation typical degradation processes occur, but their influence starts to dominate only after \sim the 30-th cycle, resulting in decreasing of capacity retention. Elevated temperature speeds up segregation of extra NiO-phase from NCM substrate particle surface and balances two effects: intrinsic capacity degradation and exploitation of electrode mass. Therefore, capacity retention of LNP-NCM_B stays at the same level (at HT) or even increases (at RT) during the first 20 cycles (Figure 2b, d).

In 1993, Ozhuk recommended to limit the deepness of charge for LiNiO₂ at level ca. 75% of the maximum lithium concentration.^[66] From Table 3, it is clear that at room temperature test this critical Li concentration limit at the first charge was not achieved only in case of LNP-NCM_B sample. Other samples broke limit of 207 mAh/g at the first delithiation process, that caused not only large capacity loss on the first cycle, but also substantial deterioration of their cycle life (mostly lower than 90% for 50 cycles) due to detrimental structure transformation. If a critical amount of de-intercalated

Li-ions is exceeded, a part of the capacity is permanently lost. Therefore, we suppose, this irreversible part of total capacity loss is the largest for LNP-NCM_W samples.

First several cycles set a scenario for further electrochemical behavior, which can be or cannot be realized depending on other material properties. Incomplete lithium extraction preserves structural degradation gained with each cycle. That is why most of coated samples have the same or lower discharge capacity as bare sample at the beginning of cycling, but better capacity retention for prolonged cycling.

Prolonged cycling of LNP-NCM_B sample shows both increased discharge capacity (comparing to other samples) and improved capacity retention, especially at elevated temperature. The positive effects of modifying by La₂(Li_{0.5}Ni_{0.5})O₄-phase was reported previously and associated to facilitating the movement of lithium ions across electrode/electrolyte interface.^[34-41]

Nevertheless, modification of washed NCM powder (with the low content of LRC) by La₂(Li_{0.5}Ni_{0.5})O₄ doesn't improve noticeably electrode material performance in terms of capacity retention. At both temperature regimes we see high rate of capacity fading for LNP-NCM_W cells, which is around 85% after 50 cycles (Figure 2c, d). We assume that concurrent formation of NiO-rock salt phase during in situ La₂(Li_{0.5}Ni_{0.5})O₄-synthesis at washed NCM surface leads to blocking lithium diffusion pathways into the bulk whereas some part of surface, purified from LRC, remains vulnerable to side reactions with electrolyte.

In order to estimate cycling performance in detail, we suggest using Δ -plots in Figure 5 as well as commonly used dependences (discharge capacity and capacity retention vs. cycle number). These plots allow to evaluate reversibility precisely and the rate of charge capacity degradation simultaneously. Based on abovementioned conclusions about barely detectable difference between four samples, derived from structural analysis, we assume that degradation processes start from the first charging and influence on cycle life overall. Here, Y-axis is absolute capacity difference in mAh/g: upper curves are absolute value of Coulombic efficiency (subtraction between charge and discharge capacity for each cycle) and the lower curves were obtained by subtraction charge capacity of the next cycle from the charge capacity of the previous cycle. The difference of two neighbor cycles discharge capacities is not presented because its trend and values can be seen from Figure 2(b, d). The first several cycles were not taken under consideration because initial cycling behavior has already described above (Table 3).

The lower curves (marked as triangles) of Δ -plots are observed mostly in the negative Y-axis area, depicting on the trend of capacity decreasing. The lines, given for every curve on Figure 5, just visualize the tendency of capacity difference (Δc) from cycle to cycle and should not be considered as trend lines. If Y-coordinates of lower curves' points are almost the same from cycle to cycle, it means linear nature of capacity fading or stabilization of degradation rate (without accelerating). This situation is inherent to non-modified NCM electrodes (bare and washed) at RT (yellow triangles on Figure 5a, c). The

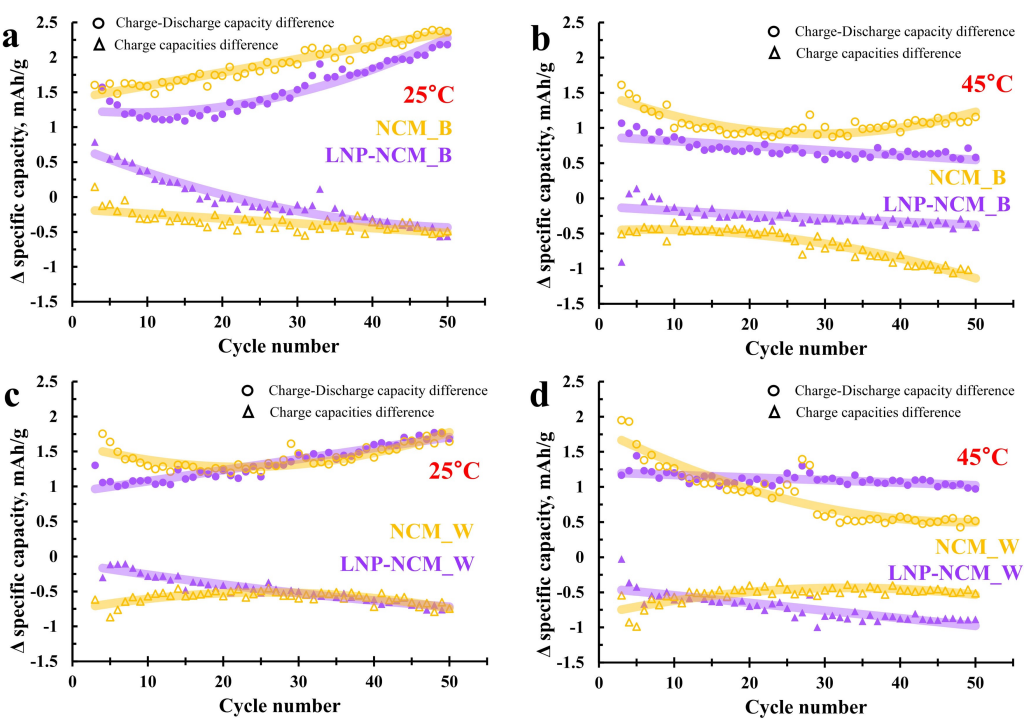


Figure 5. Δ -plots (specific capacity difference) for 1 C-cycling of NCM-based cathode materials at 3.0–4.3 V at different temperature.

rate of capacity decreasing depends on electrode material. At RT temperature for NCM_B and NCM_W (in the absence of $\text{La}_2(\text{Li}_{0.5}\text{Ni}_{0.5})\text{O}_4$ -modifying phase) almost constant rate of capacity decreasing is observed, that is reflected by horizontal curve (Figure 5a and c, yellow triangles). The stable rate of charge capacity deterioration along with gradual discharge capacity decreasing refers to reversible capacity loss, that can be recovered at special discharging conditions. It is evidence of the kinetic control of capacity fade and is related to the difference in diffusivity in charge and discharge directions. If some lower dependences are inclined, that means the accelerating of capacity fading with cycle number. It means that some irreversible transformation of structure leads to CAM loss. Notably, the two lower curves have mutual nature with upper curves, which repeat their tendency among modified and non-modified samples. It confirms that the charge deintercalation initiates degradation process. The maximum charge capacity loss does not exceed 0.7 mAh/g per 50 cycles for RT and ca. 1 mAh/g for HT regardless electrode material. All conclusions, extracted from GITT data analysis (Figure 4), are applicable here as well: at constant rate of charge capacity fading (horizontal curves on Δ -plots) gradual discharge capacity decreasing (capacity retention) is raised from retarded insertion of Li ions, which is associated with very low $D_{\text{Discharge}}$ values at highly lithiated stage. This prevents the complete accumulation of Li ions at discharge. Meanwhile, lithium extraction proceeds wholly, because of fast lithium movement at charge start point (due to high initial D_{Charge} values). The temperature rising up to 45°C weakens diffusion limitations and the difference between intercalation and deintercalation processes becomes stable (horizontal upper lines) or even decreases as in case of elevated

temperature performance of NCM_W (Figure 5d, yellow circles). Nevertheless, elevated temperature influences on NCM_B-electrodes promoting capacity degradation (Figure 5b, yellow triangles). Inclined lower curves correspond to accelerating of capacity fading and can be assigned to the lack of mobile Li^+ -ions due to irreversible reactions with electrolyte and/or appearance of surface destabilized regions, which block lithium diffusion pathway.^[24] These regions constitute a significant fragment of structure, suffered from anisotropic lattice change, formation O-depleted regions, electrolyte attacks and creation of NiO rock-salt domains. All deterioration effects are closely linked and resulted in impossibility of Li ions accumulation in some positions – CAM loss (Figure 6b). It should be noted that normally both factors of capacity degradation are present at electrode cycling with predominantly contribution of the reversible factor.

The origin of appearance of surface destabilized regions (marked by black color on Figure 6b) is Ni behavior, which plays a major role in charge compensation during the charge/discharge. As reported previously,^[67] the surface Ni undergoes incomplete oxidation during charge and demonstrates only partial reduction after discharging. It was found by different surface structural methods^[67,68] and explained by some electrochemical inactive NiO species (with rock-salt structure), presented on the surface. These rock-salt domains have already formed during the first charge and stayed for the further cycling, conditioning an irreversible contribution in total capacity loss. To emphasize the irreversible capacity loss, caused by surface destabilized regions formation, we performed separate charge/discharge experiments (Figure 7) –

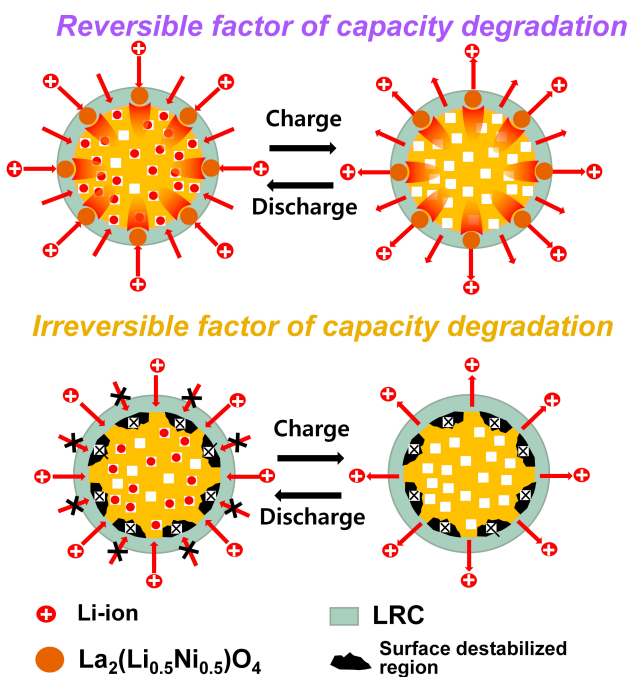


Figure 6. Illustration of capacity degradation factors for a) LNP-NCM_B and b) NCM_B.

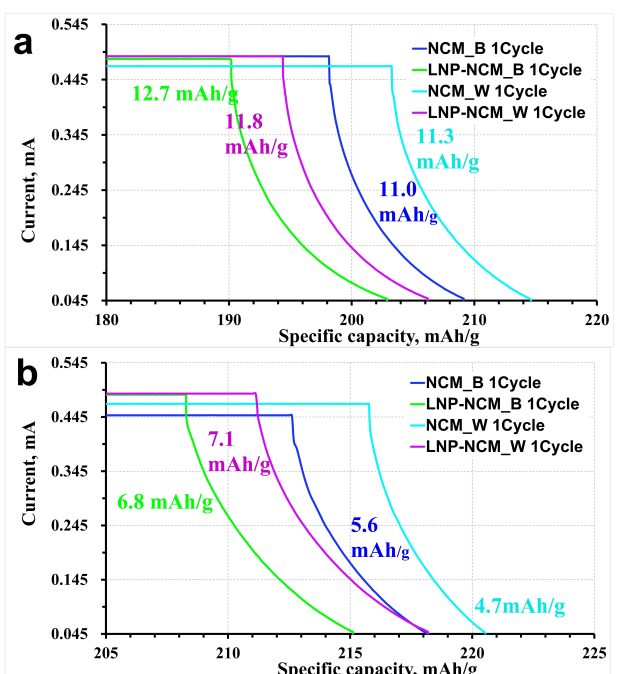


Figure 7. Current decay at constant voltage mode (CV) of discharge: a – at 25°; b – at 45 °C.

constant current (CC) discharge was combined with constant voltage (CV) discharge mode immediately after getting 3.0 V.

For this purpose, we applied additional vacuum drying (12 hours, 120 °C) for long-time storage slurry sheets at electrode preparation stage. We suppose that this step provides artificial NiO detachment and resulted in higher initial

capacity level for LNP-modified electrode set. The irreversible capacity loss was calculated by subtraction reversible discharge capacity loss (CC+CV modes) from corresponding charge capacity for each cycle (Table 4). We observed that in case of CC+CV-discharge mode irreversible capacity loss is inherent only for the first cycle at RT (for HT it is noticeable for two first cycles). But for standard cycling mode (CC discharge) this process takes places on each cycle due to incomplete, comparing to previous charge, lithium intercalation. On each next cycle new portion of Li-ions, storing from pristine bulk state, will be extracted causing more deep delithiation and more intensive structure destabilizing. The reason why LNP-modified samples have the largest irreversible capacity loss on the first cycle (around 18 mAh/g at RT and close to 10 mAh/g at HT) is explained by improving of ionic conductivity of material. As evidence, the reversible capacity loss contribution in case of LNP-modified electrodes is also the highest (~12 mAh/g for RT and ~7 mAh/g for HT), resulting from facilitating of Li-ions movements (red color zones on Figure 6a). This process intensively occurs for LNP-modified electrodes on the first cycle, but almost finished after it whereas for non-modified samples it continues for whole cycle life and leads to surface destabilization spread. So, we ascribe irreversible capacity loss to the presence of surface destabilized regions, which once formed is always localized on particles' surface. Even though very long and sparing mode will be applied for discharge direction (lithiation) no more capacity can be obtained in current cycle and no more (which is more important) capacity can be extracted in the next cycle. In other words, from CC+CV combined discharge mode it is clear that discharge capacity of previous cycle restricts the charge capacity of the next cycle in spite of existence of much more reserved lithium in cathode material (in accordance with its theoretical capacity ~280 mAh/g). Traditional battery performance test does not involve CV mode for discharging. That is why the coulombic efficiency of each cycle in ordinary cycling test is markedly less than 100% (apparent coulombic efficiency).

In our test mode (with CV discharge) the real coulombic efficiency exceeds 100%, depicted that Li-ions are readily insert into empty positions, arising from the very first cycle. From the kinetic point of view, there is no limitation to full lithium intercalation except the abnormal decreasing of D at the end of lithiation, which is mostly overcome by applying slow CV discharging mode. In some cases, the next charge capacity exceeds the previous discharge capacity because of the fact that lithium ions store is still presented in material bulk, originated from the pristine state. This phenomenon is more pronounced for LNP-NCM_B electrode – almost on 6 mAh/g extracted lithium capacity more comparing to previous amount of inserted lithium.

Moreover, from the first cycle CC-CV-combined experiment (as well as for CC-discharge test) it is evident that NCM_W material has the highest coulomb efficiency due to almost absence of high-resistive LRC-layer on particles' surface, but it does not lead to better cyclability properties (Figure 2).

The highest degradation rate is observed for LNP-NCM_W sample at HT and attributed to the destruction of protective

Table 4. Initial electrochemical performance at room and elevated temperature (0.1 C, 3.0–4.3 V). Combined discharge mode (CC + CV).

Test temperature [°C]	Sample	The 1-st cycle capacity [mAh/g]			The 2-nd cycle capacity [mAh/g]		
		Charge	Discharge CC mode	Cap.loss (revers.+irrevers.) ^[a]	Charge	Discharge CC mode	Cap.loss (revers.+irrevers.) ^[a]
25 (RT)	NCM_B	225.4	198.1	27.3 (11.0 + 16.3)	210.8	200.3	11.0 (11.0 + 0) ^[b]
	LNP-NCM_B	220.6	190.2	30.4 (12.7 + 17.7)	208.6	196.4	12.5 (12.5 + 0) ^[b]
	NCM_W	225.6	203.3	22.3 (11.3 + 11.0)	217.0	204.0	13 (11.2 + 1.8)
	LNP-NCM_W	224.6	194.4	30.2 (11.8 + 18.4)	208.8	197.5	11.6 (11.6 + 0) ^[b]
45 (HT)	NCM_B	225.0	212.6	12.4 (5.6 + 6.8)	219.9	214.4	5.5 (4.2 + 1.3)
	LNP-NCM_B	224.9	208.3	16.6 (6.8 + 9.8)	217.8	212.0	5.8 (5.1 + 0.7)
	NCM_W	227.1	215.8	11.3 (4.7 + 6.6)	222.2	215.4	6.8 (4.4 + 2.4)
	LNP-NCM_W	226.3	211.1	15.2 (7.1 + 8.1)	220.2	214.0	6.2 (5.2 + 1.0)

[a] Reversible capacity loss was obtained at constant voltage (CV) mode by registration of rest discharge current to 0.01 C value. Irreversible capacity loss was calculated by subtraction of discharge capacity (CC + CV modes) from corresponding charge capacity. [b] Zero-value means the absence of irreversible capacity loss. In discharge process inserted lithium overcompensated its extracted at corresponding charge process content.

LRC layer and surface destabilization (irreversible factor of capacity degradation) caused by washing and LNP-modification procedures (Figure 5d). In this case LNP-particles consume LRC (the rest after washing) and make part of NCM surface exposed to electrolyte attack. The lowest rate of degradation nearly without accelerating ($\approx 0.3 \text{ mAh/g} \cdot \text{cycle}$ – purple triangles on Figure 5b) is demonstrated by LNP-NCM_B sample at HT. That means LNP-modifying partly reconstructs bare NCM surface and makes LRC layer thinner at sample's preparation stage. In this case only kinetic restrictions suppress full lithiation (reversible factor of capacity degradation). On charge-discharge profiles it is reflected as decreased polarization (Figure 8b vs. a). All non-preferred surface transformation leads to rapid increasing of cell polarization, which limits lithium extraction upon cycling in addition (Figure 8d vs. c).

As discussed above the probable negative effect of co-synthesized NiO (artificially introduced) was eliminated by its peeling from NCM substrate due to elevated temperature of measurements and allowed to realize the positive effect of $\text{La}_2(\text{Li}_{0.5}\text{Ni}_{0.5})\text{O}_4$ -modifying. There is no acceleration of charge capacity decreasing (horizontal tendency of charge capacity

difference) for LNP-NCM_B-electrodes at HT and its absolute values are the smallest (less than 0.5 mAh/g per 50 cycles).

To confirm our assumption about positive influence of LNP-modification on NCM layered structure we performed *ex situ* XRD measurement of cycled and fresh electrodes of LNP-NCM_B material in comparison with non-modified NCM_B electrode. The electrodes after 50 cycles of galvanostatic measurements (from Figure 2b) as well as uncycled (fresh) electrodes were analyzed for structural stability (Figure 9). All reflections of fresh and cycled electrodes were indexed as layered $\alpha\text{-NaFeO}_2$ of R3 m space group. No more additional peaks are observed after cycling. This fact suggests that the NCM bulk structure remains stable during electrochemical cycling. However, there is (003) and (104) peaks position shifting to lower angles for cycled electrodes (arrows on Figure 9), which is significantly pronounced for NCM_B material, that is accompanied by *c*-axes expansion (on 0.24% for LNP-NCM_B and 0.36% for NCM_B) and *a*-axes shrinkage (on 0.24% for LNP-NCM_B and 0.32% for NCM_B) after repeated charging and discharging. This implies repulsion of oxygen atoms on opposing transition metal slabs and increasing interlayer distance due to lithium deficiency. As

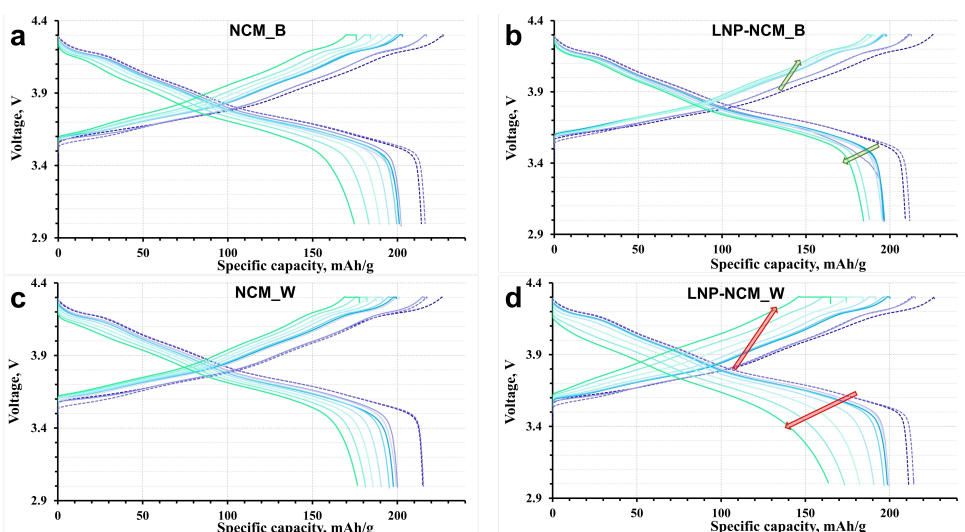


Figure 8. Charge/discharge curves evolution (at 1 C, 45 °C) with cycle number (first two formation cycles at 0.1 C marked as dashed lines). Red arrows correspond to increased polarization, green arrows – normal polarization.

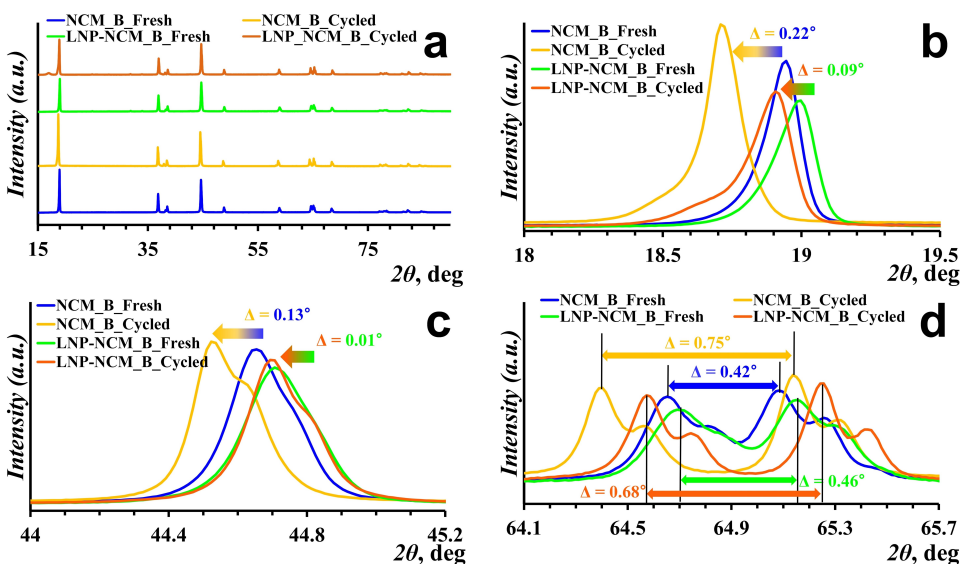


Figure 9. XRD patterns a) for all electrodes; b-d) fragments at different 2θ -ranges. The gradient color arrows show peaks shifting.

cycled electrodes was scanned at discharge state, the lattice evolution is explained by progressive irreversible removing of Li-ions from the structure. In case of LNP-modified electrodes this detrimental process is weak whereas for NCM bare material it is more obvious. The same trend we observed on the Δ -plots (Figure 5b): the accelerating of charge capacity loss for NCM_B (yellow triangles on Figure 5b) is more explicit and caused by the stronger Li-ions exhaustion, gained with each cycle. LNP-modification (purple triangles on Figure 5b) suppresses over-limit lithium depletion and supports structure stability. Moreover, NCM_B pattern shows more noticeable (108)/(110) peaks splitting than LNP-NCM_B (Figure 9d), that is complementary to observed trend.

Both phenomena: the absence of charge capacity accelerating and decreasing of resistance of LNP-NCM_B electrodes (Figure 8) refer to the thinning of CEI and confirm the

successful converting part of LRC into functional surface modifier $\text{La}_2(\text{Li}_{0.5}\text{Ni}_{0.5})\text{O}_4$, possessing high conductive properties. These two facts suggest that the presence of $\text{La}_2(\text{Li}_{0.5}\text{Ni}_{0.5})\text{O}_4$ -phase at NCM surface inherently improves its electrochemical properties but the way of modifying and its content play crucial role for electrode cycle life.

The particles' surface of samples was the object our further investigations. STEM-EDX elemental mapping illustrated that La was found to be concentrated in nano-sized particles at the edges of NCM surface grains (Figure 10). Elemental analysis from surface points shows that ratio La:Ni is close to stoichiometric as the one in $\text{La}_2(\text{Li}_{0.5}\text{Ni}_{0.5})\text{O}_4$ phase. After cycling the morphology of particles is changed: NCM_B secondary particles becomes more porous and cracks formation is distributed across the boundary of primary particles (Fig-

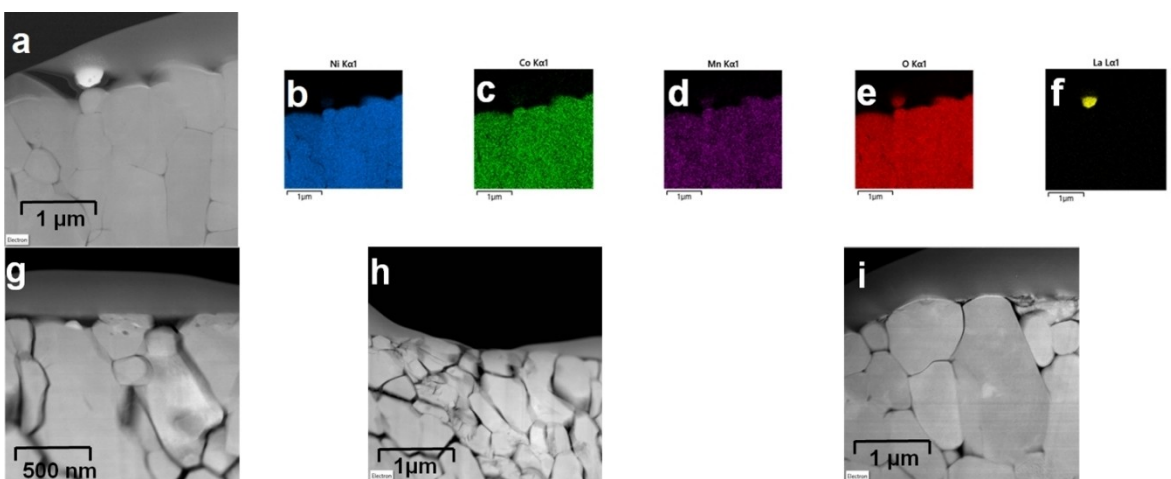


Figure 10. STEM-images of samples before cycling: a) LNP-NCM_B, i) NCM_B, and after cycling: g) LNP-NCM_B and h) NCM_B. b-f) EDS-mapping from point for uncycled LNP-NCM_B.

ure 10h). The surface area of LNP-NCM_B material looks less damaged after cycling (Figure 10g).

We used HRTEM to explore the surface structural changes of studied materials (Figure 11). Pristine NCM_B sample before cycling exhibits a highly crystalline structure with lattice fringes, extended to the surface (Figure 11b). However, NCM_B pristine powder reveals very thin rock-salt layer (Figure 11a). We supposed, during several months of storage (even in dry room condition) NCM particles' surface undergoes interaction with surrounding atmosphere, that deteriorates layered structure. After cycling at 3.0–4.3 V for 50 cycles, the bulk region of LNP-NCM_B remains as original, whereas particle's surface converts to barely detected destabilized region (~3 nm) (Figure 11d). This detrimental transformation is more significant for NCM_B cycled electrode material (~13 nm) (Figure 11c), confirming more intensive structure degradation, observed above in electrochemical experiments. The growth of rock-salt surface

layer for NCM_B after cycling supports scheme of capacity degradation factors, presented on Figure 6. LNP-modification constrains surface structure deterioration at cycling, signifying better cyclability properties.

In order to clarify the effect of LNP-modification on NCM material properties we calculated the cumulative discharge capacity for samples' sets upon cycling (Figure 12), which can be useful from practical point of view. Obviously, at elevated temperature LNP-NCM_B electrode exhibits the best capability to reversible accumulation of Li^+ ions, that plays the decisive role in further investigation of LNP-modification.

Conclusion

The initial structural data in terms of lattice parameters and cation mixing degree are not able to predict electrode's cycle

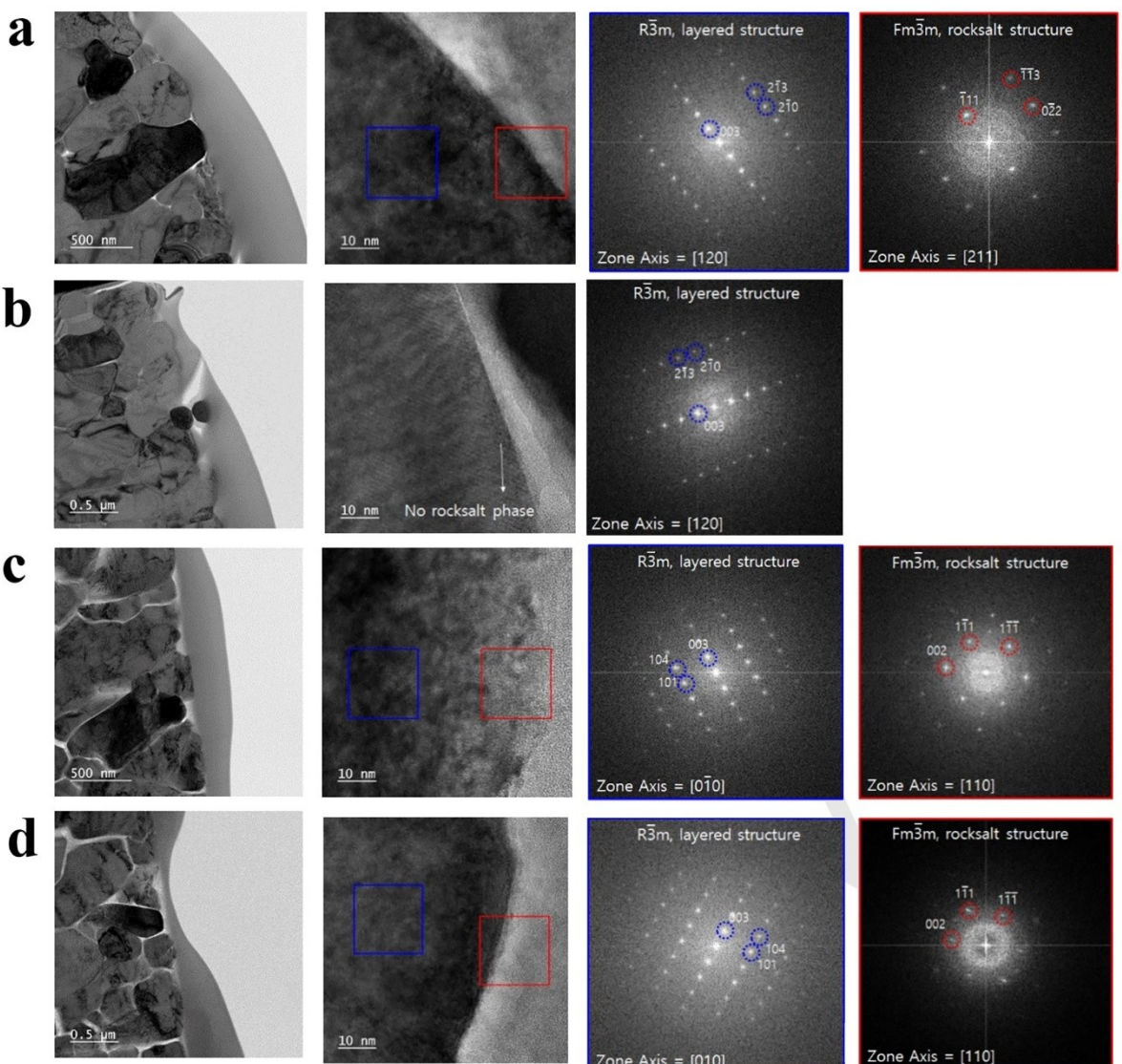


Figure 11. TEM image of a) NCM_B before and c) after cycling, b) LNP-NCM_B before and d) after cycling. HRTEM image of white region and corresponding FFT pattern (right side pictures).

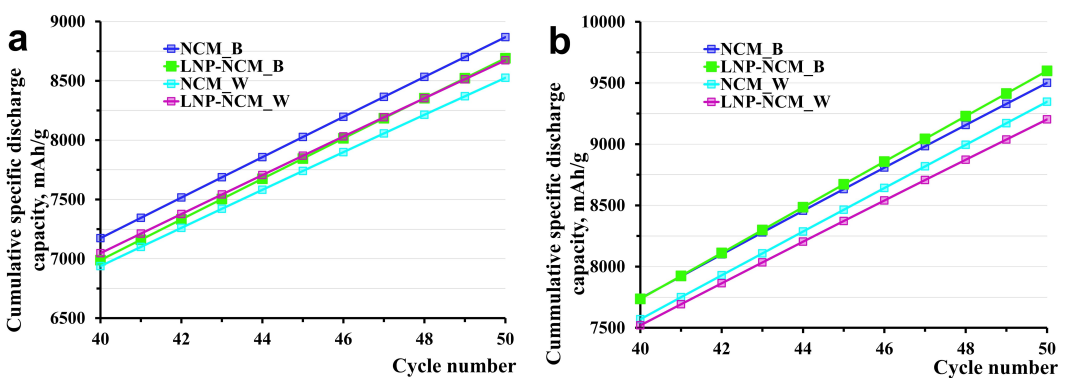


Figure 12. Cumulative specific discharge capacity, collected after 50 cycles (cycling at 1 C, 3.0–4.3 V): a) 25 °C, b) 45 °C.

life behavior. They are applicable for characterization of several initial cycles at most. The calculated data for interslab thickness is more helpful for understanding processes, occurred at the start region of galvanostatic cycling. Namely, initial charging creates preconditions for extended cycle life properties of electrodes. All deterioration processes (like formation inactive of NiO, increasing Ni/Li disordering, appearance of O-depletion region, increasing electrode polarization) originate from Li⁺ extraction, especially over critical level of lithium depletion. Combination of all effects reflects on capacity retention of cells, which cannot be predicted in advance. They can be manifested as accelerating of capacity fading or can be suppressed by some material treatment procedure (like, washing, coating, doping, reheating and so on).

In this paper we suggested to perform cycling data as Δ -plots in order to precisely evaluate the capacity degradation at cycling. It can be estimated within 50 cycles, based on differentiated dependences of charge electrode capacity. For illustration of capacity fading reasons, mainly affected on electrode cycle life, we presented the analysis of degradation rate in order to attribute constant value of capacity fading (horizontal curve) to solely reversible factor of capacity loss caused by the difference of lithium diffusivity in layered structure and accelerating of capacity fading – to irreversible factor (inclined curve), which significantly contributes in total electrode deterioration in case of modification of washed NCM material. Both factors (reversible and irreversible capacity loss) restrict NCM cycle life behavior. Surface modification converting lithium residual compounds into Li-conductive phase and providing fast Li ions transport, was found to overcome the influence of detrimental processes, occurred presumably at high operating voltage. LNP-modified NCM bare cathode material demonstrated improved electrochemical performance in terms of capacity retention and cumulative discharge capacity due to surface reconstruction by high conductive perovskite-like phase La₂(Li_{0.5}Ni_{0.5})O₄. Suggested in this work the detection of reversible and irreversible factors of capacity loss of layered oxide cathode material was supported by results of *ex situ* XRD measurements, STEM-EDS, SEM and GITT measurements, which are in good agreement.

Experimental Section

For the synthesis of electrode material samples based on LiNi_{0.85}Co_{0.10}Mn_{0.05}O₂, the following reagents were used: nickel sulfate (NiSO₄·6H₂O, 99%, Sanchun Chem.), cobalt sulfate (CoSO₄·7H₂O, 99%, Sanchun Chem.), manganese sulfate (MnSO₄·H₂O, 99%, Sanchun Chem.), sodium hydroxide (NaOH, 98%, Sanchun Chem.), lithium hydroxide (LiOH, 98%, Sanchun Chem.). Metal (Ni, Co, and Mn) sulphate solutions were mixed in the following ratio based on the elemental composition: Ni:Co:Mn = 0.85:0.10:0.05. The mixture was placed in a coprecipitation reactor, in which a mixture of Ni(OH)₂, Co(OH)₂, and Mn(OH)₂ hydroxides was precipitated by gradual addition of sodium hydroxide. The mixture was washed, the precipitate was separated, after which the precursor was placed in a device for mixing with dry LiOH in the molar ratio Li:(Ni + Co + Mn) = 1.03:1. Heat treatment (750 °C, 12 hours) was conducted in a muffle furnace with air flowing at a heating rate of 5 °C min⁻¹. Such material was used as a base and was designated NCM_B. The water washing process was made by mixing the cathode material and water 1:1 in a beaker, and the product obtained after washing was dried using a filter press. This sample was named as NCM_W.

LNP-modifying were performed in liquid media. Appropriate amounts of solid salts La(NO₃)₃·6H₂O and Ni(NO₃)₂·6H₂O (corresponds to 1% by weight in modified powder) were dissolved in distilled water and stirred with magnetic bar for 0.5 hour. We did not use purposely any lithium sources, assuming utilization of lithium residual compounds, presented on NCM particles' surface. 10 g of NCM powders (bare and washed) were added under constant stirring. After that heating were applied for water evaporation. Finishing drying took place in oven at 80 °C in dry room atmosphere overnight. Thus, processed powders were heat treated at 700 °C under O₂-flowing for 5 hours (heating rate 5 °C/min and free cooling). Ready powders (LNP-NCM_B and LNP-NCM_W) were sieved and collected in dry room for further measurements.

The studies of the LiNi_{0.85}Co_{0.10}Mn_{0.05}O₂ electrode material by X-ray diffraction were performed on a PANalytical Empyrean diffractometer using Cu K α radiation $\lambda = 1.790307 \text{ \AA}$. For *ex situ* XRD test the discharged cells were disassembled in dry room, electrodes were washed in DMC and dried under vacuum. The morphology of the LiNi_{0.85}Co_{0.10}Mn_{0.05}O₂ material was examined using a JEOL scanning electron microscope (SEM) with a W cathode and an accelerating voltage of 10 kV. The diffraction patterns were analyzed using the FullProf and WinPLOTR software package and the PDF-4 database. The background signal was defined by fitting a linear interpolation between selected data points in non-overlapping regions; NCM and LNP-phases reflections was fitted by pseudo-Voigt function. In

all cases, background, scale factor, zero point, coefficients for the peak shape function, asymmetry parameters and cell parameters were refined.

TEM specimen of cathode particles were prepared by focused ion beam (Helios 5 UC, ThermoFisher Scientific). TEM images were obtained using JEOL JEM-ARM200F (JEOL) under 200 kV with charge-coupled device (CCD, USC 1000XP, Gatan). Energy dispersive X-ray spectroscopy (EDS) point analysis and elemental maps were collected using X-Max 100TLE (Oxford Instruments). TEM specimen preparation and characterization were conducted at Research Institute of Industrial Science and Technology (RIIST).

The electrodes under study consisted of 96.5 w% $\text{LiNi}_{0.85}\text{Co}_{0.10}\text{Mn}_{0.05}\text{O}_2$, 1.5 w% Super C65 carbon black (Timcal), and 2 w% PVDF binder. The electrolyte was a solution of 1 M LiPF₆ in a mixture of ethylene carbonate : dimethyl carbonate, diethyl carbonate (3:4:5 by volume). The electrode suspension was applied to Al-foil with a deposition density of 12 mg/cm². Electrochemical measurements were conducted in sealed two-electrode coin cells with Li metal as a counter-electrode.

Cycling was started from the formation cycles. Two formation cycles were registered at 0.1 C (in combination with CV – constant voltage mode – up to current reached 0.05 C after charging). Since from the 3-rd cycle applied current loading was 1 C (for both charge and discharge directions). Separate electrochemical test was conducted in combined discharge steps: constant current discharge (0.1 C) followed by constant voltage discharge (CV) at 3.0 V up to current decreasing 0.01 C. Galvanostatic measurements were performed at room temperature (25 °C) and at elevated temperature (45 °C). All measurements were carried out in three parallel cells (marked as dots on cycle life dependences) and average meaning of capacity values is presented as solid line.

Acknowledgements

This work was supported by the Brain Pool Program (2021H1D3A2A0080284) supervised by National Research Foundation of Korea (NRF) and Material parts development business program (20016080) supervised by Korea Evaluation Institute of Industrial Technology (KEIT).

Conflict of Interest

The authors declare no conflict of interest.

Data Availability Statement

The data that support the findings of this study are available from the corresponding author upon reasonable request.

Keywords: capacity fading · capacity retention · cycle life · high Ni layered oxide · $\text{La}_2(\text{Li}_{0.5}\text{Ni}_{0.5})\text{O}_4$ perovskite-like · lithium-ion battery · irreversible capacity loss · modified cathode material

[1] A. O. Kondrakov, H. Geßwein, K. Galdina, L. de Biasi, V. Meded, E. O. Filatova, G. Schumacher, W. Wenzel, P. Hartmann, T. Brezesinski, J. Janek, *J. Phys. Chem. C* **2017**, *121*, 24381–24388.

- [2] C. Liao, F. Li, J. Liu, *Nanomaterials* **2022**, *12*, 1888–1913.
- [3] C. M. Julien, A. Mauger, *Energies* **2020**, *13*, 6363–6409.
- [4] B. Zhu, Z. Yu, L. Meng, Z. Xu, C. Lv, Y. Wang, G. Wei, J. Qu, *Ionics* **2021**, *27*, 2749–2784.
- [5] S. H. Song, M. Cho, I. Park, J.-G. Yoo, K.-T. Ko, J. Hong, J. Kim, S.-K. Jung, M. Avdeev, S. Ji, S. Lee, J. Bang, H. Kim, *Adv. Energy Mater.* **2020**, *10*, 2000521–2000531.
- [6] C.-C. Yang, P.-C. Liao, Y.-S. Wu, S. J. Lue, *Appl. Surf. Sci.* **2017**, *399*, 670–681.
- [7] S. Dong, Y. Zhou, C. Hai, J. Zeng, Y. Sun, Y. Shen, X. Li, X. Ren, G. Qi, X. Zhang, L. Ma, *Ceram. Int.* **2019**, *45*, 144–152.
- [8] V.-C. Ho, H. An, M. Hong, S. Lee, J. Kim, M. B. Park, J. Mun, *Energy Technol.* **2021**, *9*, 2000800.
- [9] S.-T. Myung, K. Izumi, S. Komaba, Y.-K. Sun, H. Yashiro, N. Kumagai, *Chem. Mater.* **2005**, *17*, 3695–3704.
- [10] S.-T. Myung, K. Izumi, S. Komaba, H. Yashiro, H. J. Bang, Y.-K. Sun, N. Kumagai, *J. Phys. Chem. C* **2007**, *111*, 4061–4067.
- [11] J.-I. Hata, M. Hirayama, K. Suzuki, N. Dupre, D. Guyomard, R. Kano, *Batteries & Supercaps* **2019**, *2*, 454–463.
- [12] M. A. Philip, R. Haasch, J. Kim, J. Yang, R. Yang, I. Kochetkov, L. F. Nazar, A. A. Gewirth, *Batteries & Supercaps* **2020**, *4*, 294–303.
- [13] D. Kitsche, F. Strauss, Y. Tang, N. Bartnick, A.-Y. Kim, Y. Ma, C. Kübel, J. Janek, T. Brezesinski, *Batteries & Supercaps* **2022**, *5*, e202100397.
- [14] K. Edstrom, T. Gustafsson, J. O. Thomas, *Electrochim. Acta* **2004**, *50*, 397–403.
- [15] W. Lee, S. Lee, E. Lee, M. Choi, R. Thangavel, Y. Lee, W.-S. Yoon *Energy Storage Mater.* **2022**, *44*, 441–451.
- [16] N. D. Phillip, B. L. Armstrong, C. Daniel, G. M. Veith, *ACS Omega* **2020**, *5*, 14968–14975.
- [17] Y. Levartovsky, X. Wu, C. Erk, S. Maiti, J. Grinblat, M. Talanker, D. Aurbach, *Batteries & Supercaps* **2020**, *4*, 221–231.
- [18] H. Gao, X. Zeng, Y. Hu, V. Tileli, L. Li, Y. Ren, X. Meng, F. Maglia, P. Lamp, S.-J. Kim, K. Amine, Z. Chen, *ACS Appl. Energ. Mater.* **2018**, *1*, 2254–2260.
- [19] M. Yoon, Y. Dong, J. Hwang, J. Sung, H. Cha, K. Ahn, Y. Huang, S. J. Kang, J. Li, J. Cho, *Nat. Energy* **2021**, *6*, 362–371.
- [20] D. Weber, D. Tripković, K. Kretschmer, M. Bianchini, T. Brezesinski, *Eur. J. Inorg. Chem.* **2020**, *2020*, 3117–3130.
- [21] B. Han, B. Key, S. H. Lapidus, J. C. Garcia, H. Iddir, J. T. Vaughney, F. Dogan, *ACS Appl. Mater. Interfaces* **2017**, *9*, 41291–41302.
- [22] S.-T. Myung, H. Amine, Y.-K. Sun, *J. Mater. Chem.* **2010**, *20*, 7074–7095.
- [23] H.-H. Ryu, K.-J. Park, C. S. Yoon, Y.-K. Sun, *Chem. Mater.* **2018**, *30*, 1155–1163.
- [24] C. Xu, K. Märker, J. Lee, A. Mahadevogowda, P. J. Reeves, S. J. Day, M. F. Groh, S. P. Emge, C. Ducati, B. L. Mehdi, C. C. Tang, C. P. Grey, *Nat. Mater.* **2021**, *20*, 84–92.
- [25] C. Delmas, J. P. Pérès, A. Rougier, A. Demourgues, F. Weill, A. Chadwick, M. Brousse, F. Perton, Ph. Biensan, P. Willmann, *J. Power Sources* **1997**, *68*, 120–125.
- [26] Y. Makimura, T. Sasaki, T. Nonaka, Y. F. Nishimura, T. Uyama, C. Okuda, Y. Itou, Y. Takeuchi, *J. Mater. Chem. A* **2016**, *4*, 8350–8358.
- [27] F. Friedrich, B. Strehle, A. T. S. Freiberg, K. Kleiner, S. J. Day, C. Erk, M. Piana, H. A. Gasteiger, *J. Electrochem. Soc.* **2019**, *166*, A3760–A3774.
- [28] A. Yano, M. Shikano, A. Ueda, H. Sakaebe, Z. Ogumi, *J. Electrochem. Soc.* **2016**, *164*, A6116–A6122.
- [29] A. V. Ivanishchev, A. V. Ushakov, I. A. Ivanishcheva, A. V. Churikov, A. V. Mironov, S. S. Fedotov, N. R. Khasanova, E. V. Antipov, *Electrochim. Acta* **2017**, *230*, 479–491.
- [30] A. V. Ivanishchev, I. A. Ivanishcheva, A. Dixit, *Russ. J. Electrochem.* **2019**, *55*, 719–737.
- [31] J. Kim, H. Cha, H. Lee, P. Oh, J. Cho, *Batteries & Supercaps* **2019**, *3*, 309–322.
- [32] M. Jiang, D. Danilov, R.-A. Eichel, P. H. L. Notten, *Adv. Energy Mater.* **2021**, *11*, 2103005–2103049.
- [33] L. Liu, M. Li, L. Chu, B. Jiang, L. Ruoxu, Z. Xiaopei, G. Cao, *Prog. Mater. Sci.* **2020**, *111*, 100655–100740.
- [34] A. Yasmin, M. A. Shehzad, J. Wang, X.-D. He, X. Ding, S. Wangi, Z. Wen, C. Chen, *ACS Appl. Mater. Interfaces* **2020**, *12*, 826–835.
- [35] A. Yasmin, M. A. Shehzad, X. Ding, J. Wang, R. Yu, M. Deng, Z. Tang, C. Chen, *J. Alloys Compd.* **2020**, *827*, 153208–153217.
- [36] K. Heo, J. Lee, J. Im, M.-Y. Kim, H.-S. Kim, D. Ahn, J. Kim, J. Lim, *J. Mater. Chem. A* **2020**, *8*, 22893–22907.
- [37] C. Sengottaiyan, K. Kubota, S. Kumakura, Y. TaeHyeon, T. Hosaka, S. Komaba, *J. Electrochem. Soc.* **2021**, *168*, 110505–110513.
- [38] L. Li, L. Fu, M. Li, C. Wang, Z. Zhao, S. Xie, H. Lin, X. Wu, H. Liu, L. Zhang, L. Tan, *J. Energy Chem.* **2022**, *71*, 588–594.

- [39] J. Zhou, Z. Han, Y. Zhang, A. Zhu, X. He, H. Wu, X. Chen, Q. Wang, Y. Zhang, *J. Mater. Chem. A* **2021**, *9*, 3427–3441.
- [40] R. Zhang, Y. Wang, X. Song, G. Li, S. Liu, X. Gao, *ChemElectroChem* **2020**, *7*, 2042–2047.
- [41] F. Wu, Q. Li, L. Chen, Q. Zhang, Z. Wang, Y. Lu, L. Bao, S. Chen, Y. Su, *ACS Appl. Mater. Interfaces* **2019**, *11*, 36751–36762.
- [42] H. Yang, H.-H. Wu, M. Ge, L. Li, Y. Yuan, Q. Yao, J. Chen, L. Xia, J. Zheng, Z. Chen, J. Duan, K. Kisslinger, X. C. Zeng, W.-K. Lee, Q. Zhang, J. Lu, *Adv. Funct. Mater.* **2019**, *29*, 1808825–1808838.
- [43] J. Zheng, Y. Ye, T. Liu, Y. Xiao, C. Wang, F. Wang, F. Pan, *Acc. Chem. Res.* **2019**, *52*, 2201–2209.
- [44] S. Xu, X. Wang, W. Zhang, K. Xu, X. Zhou, Y. Zhang, H. Wang, J. Zhao, *Solid State Ionics* **2019**, *334*, 105–110.
- [45] D. Mohanty, H. Gabrisch, *J. Power Sources* **2012**, *220*, 405–412.
- [46] P. Teichert, G. G. Eshetu, H. Jahnke, E. Figgemeier, *Batteries* **2020**, *6*, 6010008–6010034.
- [47] Y. Cho, P. Oh, J. Cho, *Nano Lett.* **2013**, *13*, 1145–1152.
- [48] G. Sun, X. Yin, W. Yang, A. Song, C. Jia, W. Yang, Q. Du, Z. Ma, G. Shao, *Phys. Chem. Chem. Phys.* **2017**, *19*, 29886–29894.
- [49] N. V. Faenza, L. Bruce, Z. W. Lebens-Higgins, I. Plitz, N. Pereira, L. F. J. Piper, G. Amatucci, *J. Electrochem. Soc.* **2017**, *164*, A3727–A3741.
- [50] B. Huang, D. Liu, K. Qian, L. Zhang, K. Zhou, Y. Liu, F. Kang, B. Li, *ACS Appl. Mater. Interfaces* **2019**, *11*, 14076–14084.
- [51] Y. Zhou, Z. Hu, Y. Huang, Y. Wu, Z. Hong, *J. Alloys Compd.* **2021**, *888*, 161584–161590.
- [52] L. You, B. Chu, G. Li, T. Huang, A. Yu, *J. Power Sources* **2021**, *482*, 228940–228949.
- [53] Y. Li, H. Shi, J. He, X. Li, Z. Chen, Y. Zhang, L. Deng, P. Dong, D. Wang, Y. Zhang, J. Duan, *Appl. Surf. Sci.* **2022**, *593*, 153409–153418.
- [54] L. Hartmann, D. Pritzl, H. Beyer, H. A. Gasteiger, *J. Electrochem. Soc.* **2021**, *168*, 070507–070517.
- [55] D. Pritzl, T. Teufel, A. T. S. Freiberg, B. Strehle, J. Sicklinger, H. Sommer, P. Hartmann, H. A. Gasteiger, *J. Electrochem. Soc.* **2019**, *166*, A4056–A4066.
- [56] S. P. Kühn, K. Edström, M. Winter, I. Cekic-Laskovic, *Adv. Mater. Interfaces* **2022**, *9*, 2102078–2102094.
- [57] G. Zampardi, F. La Mantia, *Batteries & Supercaps* **2020**, *3*, 672–697.
- [58] U. Nisar, N. Muralidharan, R. Essehli, R. Amin, I. Belharouak, *Energy Storage Mater.* **2021**, *38*, 309–328.
- [59] K. Park, J.-H. Park, S.-G. Hong, B. Choi, S. Heo, S.-W. Seo, K. Min, J.-H. Park, *Sci. Rep.* **2017**, *7*, 44557–44567.
- [60] J. P. Peres, C. Delmas, A. Rougier, M. Broussely, F. Perton, P. Biensan, P. Willmann, *J. Phys. Chem. Solids* **1996**, *57*, 1057–1060.
- [61] H. Zhou, F. Xin, B. Pei, M. S. Whittingham, *ACS Energy Lett.* **2019**, *4*, 1902–1906.
- [62] S.-H. Kang, W.-S. Yoon, K.-W. Nam, Z.-Q. Yang, D. P. Abraham, *J. Mater. Sci.* **2008**, *43*, 4701–4706.
- [63] J. Kasnatscheew, M. Evertz, B. Streipert, R. Wagner, R. Klöpsch, B. Vortmann, H. Hahn, S. Nowak, M. Amereller, A.-C. Genrschev, P. Lamp, M. Winter, *Phys. Chem. Chem. Phys.* **2016**, *18*, 3956–3965.
- [64] T. Kawaguchi, K. Fukuda, K. Tokuda, M. Sakaida, T. Ichitsubo, M. Oishi, J. Mizuki, E. Matsubara, *Phys. Chem. Chem. Phys.* **2015**, *17*, 14064–14070.
- [65] J. Yang, Y. Chen, Y. Li, S. Deng, S. Chang, G. Cao, D. Zhang, S. Wang, W. Li, *Mater. Chem. Phys.* **2020**, *249*, 123135–123143.
- [66] T. Ohzuku, A. Ueda, M. Nagayama, *J. Electrochem. Soc.* **1993**, *140*, 1862–1870.
- [67] S. Liu, L. Wang, C. Zhang, B. Chu, C. Wang, T. Huang, A. Yu, *J. Power Sources* **2019**, *438*, 226979–226986.
- [68] S. Hwang, S. M. Kim, S.-M. Bak, K. Y. Chung, W. Chang, *Chem. Mater.* **2015**, *27*, 6044–6052.

Manuscript received: October 25, 2022

Revised manuscript received: December 7, 2022

Accepted manuscript online: December 22, 2022

Version of record online: January 18, 2023